41. GNSS Time and Frequency Transfer

Pascale Defraigne

Time and navigation are intimately linked and rely on each other. Global navigation satellite system (GNSS) positioning is based on the measurement of time intervals needed by the signal to travel from satellites to the receiving station on the Earth or nearby. The precision of GNSS positioning is reached thanks to atomic frequency standards onboard the satellites and the possibility to determine their synchronization differences at the subnanosecond level. Time is thereby the core of GNSS. Inversely GNSS is widely used for accurate time and frequency dissemination, as well as for the comparison of distant clocks as needed for time and frequency metrology. All these aspects of using GNSS for time/frequency applications will be presented in this chapter.

41.1 GNSS Time and Frequency Dissemination

As already mentioned in Chap. 19, the basis of the global navigation satellite system (GNSS) measurements is the time interval between the emission (satellite) and reception (receiver) of the pseudorandom noise (PRN) codes. The emission time $t_e(\text{sat})$ is read in the satellite clock, while the reception time $t_r(\text{rec})$ is read in the receiver clock. The pseudorange measurement can be denoted as

$$P = c(t_r(\text{rec}) - t_e(\text{sat})) \,, \tag{41.1}$$

where c is the velocity of light. The satellite clock and the receiver clock being not synchronized, the synchronization error $(t_{\text{rec}} - t_{\text{sat}})$ between those clocks must be taken into account to get the true time interval $(t_r - t_e)$ between the emission and reception, as if it was measured with a same clock

$$(t_r(\text{rec}) - t_e(\text{sat})) = (t_r - t_e) + (t_{\text{rec}} - t_{\text{sat}}) + \text{errors} \,. \tag{41.2}$$

The true travel time $(t_r - t_e)$ multiplied by the velocity of light corresponds to the true distance between the satellite and the receiver. The pseudorange (41.1) can then be expressed as the sum of a distance, a clock synchronization error, and additional errors mainly due to atmospheric delays, multipath and noise, and hardware delays

$$P = \|\boldsymbol{x}_s - \boldsymbol{x}_r\| + c(t_{\text{rec}} - t_{\text{sat}}) + \text{errors} \,. \tag{41.3}$$

This equation contains four unknowns, three for the position and one additional which is the synchronization error $(t_{\text{rec}} - t_{\text{sat}})$ between the satellite and the receiver clocks. The fundamental of GNSS is to combine observations from several satellites to solve for these four unknowns. However, as the clocks carried by different satellites are not perfectly synchronized, the quantity $(t_{\text{rec}} - t_{\text{sat}})$ is different for all satellites and the total number of unknowns would be $3 + k$, where k is the number of satellites observed at a given epoch. The system

could therefore not be solved. For this reason, the GNSS maintains a reference time scale and provides in the navigation message the quantity $(t_{sat} - t_{ref})$ which is the synchronization error of the satellite clocks with respect to this reference. Equation (41.3) hence can be decomposed as follows

$$P = \|\boldsymbol{x}_s - \boldsymbol{x}_r\| + c(\Delta t_{rec} - \Delta t_{sat}) + \text{errors} , \qquad (41.4)$$

where $\Delta t_{sat} = (t_{sat} - t_{ref})$ is known from the navigation message and $\Delta t_{rec} = (t_{rec} - t_{ref})$ is the synchronization error between the receiver clock and the reference time scale of the GNSS. With this formulation (41.4), Δt_{rec} is the same unknown for all satellites observed at a given epoch, so that the number of unknowns is always four at any time, and the user can determine them continuously provided that a minimum of four satellites are simultaneously visible.

The reference time scale *ref* depends on the satellite clock products used. It is the reference time scale of the constellation when using the broadcast navigation messages, but various time scales are used as references in postprocessed products like those provided by the International GNSS Service (IGS) community (Chaps. 33 and 34).

For all timing applications, the most important information here is $\Delta t_{rec} = (t_{rec} - t_{ref})$, the synchronization error between the receiver and the reference. Getting this quantity for two receivers at a same epoch, whatever the distance between them, provides the difference between the two receiver clocks $(t_{rec,1} - t_{rec,2})$ at that epoch (Sect. 41.2). The present section is dedicated to the time information disseminated by the GNSS, allowing any user to get an accurate time and/or frequency.

41.1.1 Getting UTC from GNSS

Among the various procedures existing for time dissemination, GNSS is certainly the most popular when a submillisecond precision is required. It is for example extensively used for precise time tagging [41.1], banking, synchronization of communication and telecommunication networks [41.2], or the phase synchronization energy transport and distribution networks [41.3]. Each base station of the network being synchronized continuously on the accurate time disseminated by the GNSS satellites, this assures the synchronization between all the base stations.

The basis of any official time in the world is the Universal Time Coordinated (Chap. 2); local time and legal time can be directly obtained by adding the time zone corrections to Coordinated Universal Time (UTC). Each of the GNSS provides in its navigation message a second degree polynomial modeling the evolution of the difference between its reference time scale and a prediction of UTC. Combining this quantity with the Δt_{rec} estimated from the GNSS code measurements gives at each observation epoch the synchronization error between the receiver clock and the prediction of UTC

$$(t_{rec} - t_{ref}) + (t_{ref} - \text{UTC}) = (t_{rec} - \text{UTC}) . \qquad (41.5)$$

This synchronization error can then be applied to the receiver internal clock time to produce a 1 pulse per second (pps) signal synchronized continuously with this prediction of UTC.

It must be noted that the true UTC does not exist in real time. It is indeed computed monthly in postprocessing by the International Bureau of Weight and Measurements (BIPM, Chap. 2). As a consequence, any user requiring precise timing information in real time can only rely on a prediction of UTC. The best predictions of UTC are realized by the time laboratories whose clocks are contributing to the clock ensemble providing UTC. These laboratories maintain a local realization of UTC, named UTC(k) where k is the acronym of the laboratory. After each month, when UTC is computed, the BIPM reports about the differences between each prediction UTC(k) and the true UTC, and their statistical uncertainties; this information is available freely on the BIPM website. This assures the traceability of all the UTC(k) realizations. BIPM recommends that all the UTC(k) realizations be maintained at less than 100 ns of UTC, but a good proportion of laboratories reach the level of some nanoseconds, as illustrated in Fig. 41.1 which shows two examples of UTC realizations, namely UTC (PTB) and UTC (United States Naval Observatory (USNO)), where PTB is the German National Metrology Institute, and USNO is the US Naval Observatory.

Each of the GNSS constellations relies on its own reference time scale and disseminates its own prediction of UTC, which is UTC(USNO) for the Global Positioning System (GPS), UTC(SU) for the Russian Global Navigation Satellite System (GLONASS), an average of five European UTC(k)'s for Galileo and UTC(NTSC) for BeiDou, where NTSC is the National Time Service Center in China. Also Quasi-Zenith Satellite System (QZSS) is providing a link to the prediction UTC(NICT) realized by the National Institute of Information and Communications Technology in Japan. As the link to UTC should be available in real time for the users, it is broadcast as a prediction to be used till the next update. Except for GLONASS, these predictions of UTC are broadcast worldwide with an uncertainty of only a few nanoseconds. This is not the

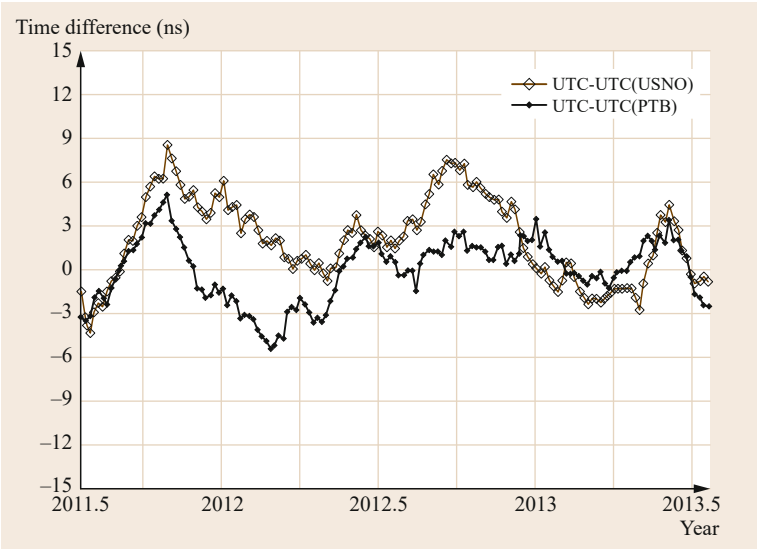

Fig. 41.1 Differences between UTC and the realizations UTC (USNO) and UTC (PTB) over 2 years

case for GLONASS, limited by an uncertainty of hundreds of nanoseconds, but it is likely to be improved in the near future through appropriate calibrations. Since January 2011, the BIPM publishes in Sect. 41.5 of its circular T values of [UTC–UTC(USNO)_GPS] and [UTC–UTC(SU)_GLONASS], that is, the differences between the true UTC and the predictions broadcast by GPS and GLONASS, respectively; during the 2 year period corresponding to Fig. 41.1, the differences [UTC–UTC(USNO)_GPS] remained within $[-12, 12]$ ns, while the differences [UTC–UTC(SU)_GLONASS] varied within $[-440, -240]$ ns.

At the user level, an accuracy of some nanoseconds on the prediction of UTC can thus presently be obtained only with GPS; Galileo and BeiDou will offer the same capability in the near future. However, the nanosecond accuracy can only be reached if the signal delays in the antenna, cable, and receiver are known; these delays reach the level of hundreds of nanoseconds, so that without any calibration of the receiving chain, GNSS can provide an access to UTC with a submicrosecond accuracy. Calibration aspects will be detailed in Sect. 41.3.2.

The accuracy statement here above should be understood within the way the uncertainties are defined for time dissemination and time transfer. As recommended in the guide to the expression of uncertainty in measurement produced by the working group 1 of the Joint Committee for Guides in Metrology [41.4], a distinction is made between the type A and type B uncertainties. The precision is given by the type A uncertainty u_A, which corresponds to the statistical uncertainty, evaluated by taking into account the level of phase noise in the raw data and the magnitude of effects varying over a typical duration below one month [41.5]; the type B uncertainty u_B is the uncertainty of the calibration. The uncertainties u_A and u_B correspond to the variance and bias in a classical decomposition of the mean-square-error. The accuracy of time measurements is then given by the combined uncertainty

$$u = \sqrt{u_A^2 + u_B^2}.$$

41.1.2 GNSS Disciplined Oscillators

For all applications requiring precise and stable frequencies, the expensive purchase of an atomic clock can be substituted by the use of a GNSS-disciplined oscillator (GNSSDO in what follows), for which the cost is much less than cesium standards.

As explained in the previous section, GNSS signals allow one to determine continuously the synchronization error between the local receiver clock and the prediction of UTC, with an accuracy of 1 μs or better, and a precision of a tens of nanoseconds. The GNSS receiver can therefore output a 1 pps signal synchronized continuously with one of the best available realizations of UTC. Considering a precision of 10 ns on the timing, it is theoretically possible to reach a frequency stability of $1 \cdot 10^{-13}$ at an averaging time of one day.

The principle of GNSSDOs (Fig. 41.2) is to generate time and frequency signals using a voltage-controlled oscillator (VCO), which can be a high-quality quartz or a rubidium oscillator, and whose frequency is controlled by timing information broadcast by the GNSS satellites and reproduced by the

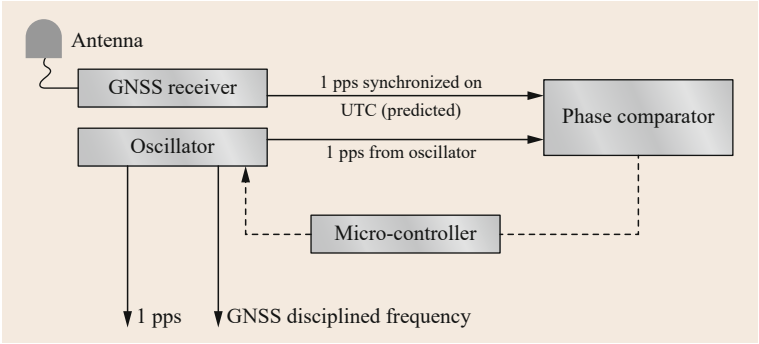

Fig. 41.2 Schematic representation of the GNSS-disciplined oscillator

GNSS receiver in its 1 pps output. The local oscillator is controlled with a servo loop, in a similar way as a phase-locked loop (PLL, see Chap. 13). In its basic form, the PLL compares the phase of the reference signal given by the GNSS receiver to the phase of the oscillator. The phase detector then outputs the phase difference between the two input signals, and a microcontroller sends the correction to be applied to the oscillator to be aligned with the GNSS received signal. In some cases, the software used by the microcontroller compensates for not only the phase and frequency changes of the local oscillator, but also for the effects of aging, temperature, and other environmental parameters [41.6]. These effects being modeled can still be corrected for in the case of temporary interruption of GNSS signals.

The software also provides the ability to vary its time constant. For example, if a more stable oscillator is used, the software can adapt the servo loop to use a longer time constant and make frequency corrections less often. Indeed, thanks to their permanent synchronization with UTC, GNSS receivers have excellent long-term stability at averaging times greater than several hours. However, their short-term stability is degraded by the noise in GNSS signals, due to multipath, atmospheric perturbations, and uncertainties in orbit and clocks broadcast in the navigation message, conferring a precision of about 30 ns on the 1 pps. On the other hand, a rubidium or a good quality quartz oscillator (like an oven-controlled oscillator) has better short term stability but is susceptible to long-term effects like aging. A GNSSDO aims at using the best of both sources, combining the short-term stability performance of the oscillator with the long-term stability of the GNSS signals to give a reference source with excellent overall stability characteristics. The time constant of the steering is therefore chosen as a function of the stability of the oscillator, compared to the stability of the GNSS-based frequency.

An illustration is provided in Fig. 41.3 which presents the Allan deviation (giving the frequency stability of the signal on different averaging times, as defined in Chap. 5) of two distinct oscillators in comparison with the Allan deviation of the GNSS-based timing signals (solid line). A time constant of about 1 h would be chosen for the illustrated oven-controlled crystal oscillator (OCXO) as for longer averaging times the GNSS-based frequency has a better stability. For the Rubidium oscillator, a time constant of about one day would be preferred to keep the frequency stability of the oscillator for shorter averaging times as it is there better than the stability of the GNSS-based frequency. For long averaging times, the GNSSDO is always based on the GNSS-based frequencies, whatever the oscillator used.

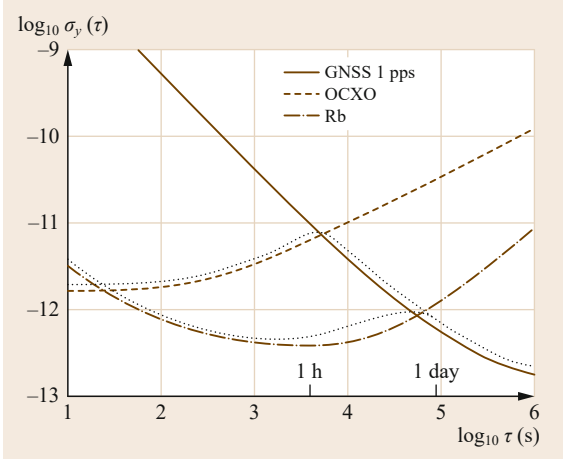

Fig. 41.3 Frequency stability of the GNSSDO for two distinct types of oscillators. The *solid line* corresponds to the Allan deviation of the GNSS, *dashed lines* to the Allan deviation of the oscillators, and *dotted lines* correspond to the Allan deviation of the frequency delivered by the GNSSDO. The GNSS 1 pps frequency stability is based on a 1 pps precision of about 30 ns

The performances of GNSSDOs are highly variable among the available models, as influenced by the design characteristics, by the oscillator implemented, by

the number of frequencies measured by the receiver (dual-frequency receiver allowing for ionospheric delays correction), etc. However, any GNSSDO that is locked to the satellite signals should be able to provide, when averaging for periods of several days or longer, a frequency accuracy at the level of some parts in 10^{13}. GNSSDO indeed rely on the GNSS predictions of UTC, and hence provide an accurate frequency (i. e., in agreement with the SI second realized by the UTC), and a long-term stability better than any free running oscillator, including the atomic standards.

GNSSDO are nowadays widely used as primary standards in calibration laboratories. They can theoretically assure the traceability of generated time and frequency to the SI second realized by UTC. Here, traceability of a measurement to the SI unit is defined as maintaining an unbroken chain of calibrations that trace back to the SI unit. GNSSDO serve as self-calibrating standards that should not require adjustment or calibration. The uncertainties on the time and frequencies generated by the GNSSDO can be determined using firstly the uncertainty of the GNSS measurements, and secondly the differences between the predicted UTC and the true UTC, as published in the BIPM Circular T. Additionally, all signal delays in internal circuits and antenna as well as their uncertainties should be determined if the GNSSDO is used as a time reference. However, as the rules for traceability vary from country to country, it is recommended to the users to refer to their national metrology institute.

41.2 Remote Clock Comparisons

People are familiar with the saying *if you have one clock you always know what time it is, but if you have more than one, you never know*! But in reality, if you have only one clock, you cannot know anything about its accuracy unless you compare it with a second clock whose you know the accuracy, and similarly for their frequency stability; furthermore if your clock suddenly stops to run, you loose completely any time information. This is the reason why it is always recommended to work with several clocks, to monitor continuously the differences between their readings and an accurate time available somewhere. Atomic clock comparisons are also essential for the needs of time and frequency metrology. First, for the generation of UTC, the only data that can be used for clocks are the differences between two clocks at successive epochs. The ensemble algorithm used to produce UTC, or any other time scale, treats therefore the differences between all the clocks of the ensemble. Second, in order to determine the frequency accuracy and the frequency stability of commercial or experimental clocks, these must be compared with other clocks whose frequency accuracy and/or stability is at least the same as the one of the clock examined. Finally, clock comparisons can be necessary for scientific applications requiring a measurement of a time interval of which the starting and closing points are measured with different clocks. This is, for example, the case for the measurement of the velocity of the neutrinos [41.7] where the clock measuring the departure time and the clock measuring the arrival time are separated by some hundreds of kilometers.

In a local environment, clocks can be compared using a phase or frequency comparator, or a time interval counter, while for remote clocks separated by some to thousands of kilometers other techniques must be envisaged. A prime requisite is that the methods of comparison at a distance do not contaminate the frequency stability of the clocks. For applications requiring only a moderate precision (some hundredths of a second), any clock can be compared to the precise time delivered by some precise time facility via the internet and the network time protocol, an internet-based hierarchical time transfer technique [41.8], or to the timing signals delivered by some radio-frequency emitting station connected to a UTC(k) realization. However, these precisions are often insufficient and the use of satellite systems is necessary; one of them is the GNSS.

41.2.1 The GNSS Time Transfer Technique

The technique, called GNSS time transfer, was used since the 1980s for the comparisons of remote frequency standards needed for the realization of UTC [41.9]. Additionally, as a consequence of its reduced cost, the technique is widely used by private companies offering time stamping, or time and frequency calibration. They then continuously monitor their local clock against the realization of UTC maintained by their national metrology institute.

GNSS time transfer is based on the following principle illustrated in Fig. 41.4. The first step is to determine the synchronization error between the local clock and the reference time scale of the GNSS. This is achieved by connecting each clock to a GNSS receiver, in such a way that the synchronization error between the internal receiver clock and the external clock can be continuously measured. From the GNSS signals, each receiver determines

$$\Delta t_{\mathrm{rec},i} = (t_{\mathrm{rec},i} - t_{\mathrm{ref}})$$

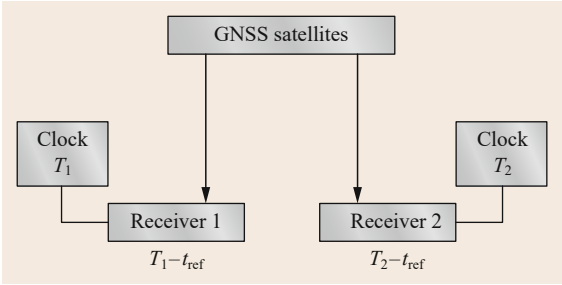

Fig. 41.4 Schematic principle of GNSS time transfer, that is, remote clock comparison

as explained in Sect. 41.1, and from the external measurement between the receiver and the clock T one gets in each laboratory

$$(T_i - t_{ref}) = (t_{rec,i} - t_{ref}) - (t_{rec,i} - T_i) \; . \qquad (41.6)$$

The second step consists in computing the difference between the quantity $(T_i - t_{ref})$ obtained in two stations $(i = 1, 2)$ from simultaneous observations to get $(T_1 - T_2)$, that is, the synchronization error between the two remote clocks. Note that in the present case simultaneous means that the two observation epochs should not differ by more than one microsecond, which can be easily reached with any GNSS receiver.

In what follows, different analysis strategies as well as the instrumental setup and requirements needed to enable a stable and accurate time and frequency transfer are discussed.

41.2.2 Time Transfer Standard CGGTTS

As timing information can only be provided by the GNSS code measurements, due to the ambiguities inherent to the carrier-phase data, the most employed time transfer tools are based on code measurements only. Carrier-phase data however provide high precision frequency comparisons, and the use of precise point positioning (Chap. 25) for time transfer is currently widespread (Sect. 41.2.4), and used for the computation of UTC since 2009 [41.10].

The common GNSS generic time transfer standard (CGGTTS) has been developed by the Consultative Committee of Time and Frequency (CCTF) as a common format to facilitate the data exchange for time dissemination and time transfer. The last version V2E [41.11] covers the use of GPS, GLONASS, Galileo, BeiDou, and QZSS and has evolved from an earlier GPS-only standard. CGGTTS files contain, among other associated quantities, the differences between the clock connected to the GNSS receiver and the GNSS reference time scale $(T - t_{ref})$. These differences result from a well-defined analysis procedure of code measurements [41.12] in which the station coordinates are fixed and the satellite position and satellite clock are extracted from the broadcast navigation messages. The computation procedure applies to satellite tracks of 13 min. For each satellite visible during this 13 min period, the corresponding solution $(T - t_{ref})$ is reported in the CGGTTS file. The tracking schedule is distributed by the BIPM as a list of the starting epochs of the tracks. Note that this 13 min duration was decided in the 1980s as it was the time required by a receiver to acquire a full GPS navigation message.

The common-view method was proposed in the 1980s by *Allan* and *Weiss* [41.9] and the associated CCTF format was based on one-channel C/A code receivers. Following the improvements of atomic frequency standards in terms of precision and accuracy, GPS (or more generally GNSS) time and frequency transfer underwent major evolutions both at the algorithmic levels and at the hardware level. A first improvement was found in the use of a multichannel approach [41.13], increasing the number of satellites which reduces correspondingly the noise of clock solutions. For applications requiring the highest precision, as for example the computation of international atomic time (TAI, Chap. 2), the CGGTTS results are improved by adding a correction for satellite orbits and clocks using the rapid IGS products. Also, the ionospheric correction used in the CGGTTS results, based on the broadcast ionospheric model of the constellation, is replaced by a new estimation based on IONosphere map EXchange format (IONEX) maps (Annnex) delivered by the IGS [41.14]. A further upgrade of the CGGTTS was the use of dual-frequency receivers measuring the GPS P(Y)-codes, enabling to remove the ionosphere delays at the first order, and leading to a factor-of-2 improvement in the precision of the intercontinental time links [41.15]. Note that for short baselines, the increase of noise in the ionosphere-free combination with respect to the single-frequency time transfer solution can be larger than the residual ionospheric errors associated with the Klobuchar model or with the IONEX maps. The same ionospheric delay is indeed suffered by the GNSS signals when they arrive in stations close to each other. However, the timing community is preferring using the ionosphere-free combination so that the CGGTTS files can be used easily whatever the distance of the second clock entering into the comparison may be.

An example of CGGTTS file is shown in Fig. 41.5. The header of the file summarizes the station information, that is, receiver name, station coordinates, and hardware delays (Sect. 41.3.2) used for the com-

```
CGGTTS     GENERIC DATA FORMAT VERSION = 2E
REV DATE = 2015-02-20
RCVR = RRRRRRRRR
CH = 12
TMS = IIIIIIIII
LAB = ABC
X = +4027889.79 m
Y =  +306995.67 m
Z = +4919491.36 m
FRAME = ITRF
COMMENTS = NO COMMENTS
INT DLY =   53.9 ns (GPS P1),   49.8 ns (GPS P2)     CAL_ID = lnnn-yyyy
CAB DLY =  200.0 ns
REF DLY =  120.6 ns
REF = UTC(ABC)
CKSUM = 3B

SAT CL  MJD  STTIME TRKL ELV AZTH   REFSV      SRSV     REFSYS    SRSYS  DSG IOE MDTR SMDT MDIO SMDI MSIO SMSI ISG FR HC FRC CK
            hhmmss  s  .1dg .1dg    .1ns     .1ps/s     .1ns    .1ps/s .1ns     .1ns.1ps/s.1ns.1ps/s.1ns.1ps/s.1ns
G24 FF 57000 000600  780 317  394    +1186342     +0         163     +0   40  12  141  +22   23   -1   23   -1  29 +2  0 L3P 5C
G05 FF 57000 000600  780  70 2325      +22617     +6         165     -3   53  26  646 +606  131   -9  131   -9  37 +1  0 L3P 8C
G17 FF 57000 000600  780 509 1217    -1407831    -36         154    -54   20  31  100   -8   24   +0   24    0  13 +4  0 L3P 7A
G16 FF 57000 000600  780 300 3022     +308130    -18         246    -28   29  41  134  -22   63   +4   63    4  21 -1  0 L3P 80
```

Fig. 41.5 Example of CGGTTS file

putation. The results are then provided, with each line corresponding to one satellite 13 min track. The columns for the time transfer solutions are REFSV and REFSYS, that is, the differences modulo one second between the laboratory clock and the satellite in view (SV) or the system time scale (SYS). They correspond to the midpoint of a linear fit applied to the 13 min results; the standard deviations with respect to this linear term are also provided (columns SRSV and SRSYS).

41.2.3 Common View or All-in-View

The initial CGGTTS files were produced by single channel receivers and the time transfer was computed as the differences of the CGGTTS results collected simultaneously from the same satellite by the two stations. The technique received the name of GPS common view (as at that time only GPS was used). All the satellite hardware delays or satellite clock errors are removed by this technique; the remaining errors are mainly due to different atmospheric distributions on the signals received at the remote stations, and the multipath at the stations. This common view (CV in what follows) technique was also used when multichannel receivers entered into the time laboratories. The final time transfer solution for the clocks T_1 and T_2 is then for each 13 min track of the BIPM schedule, a weighted average of the results obtained with the satellites in common view of both stations

$$(T_1 - T_2)(t) = \frac{1}{N(t)} \sum_{i=1}^{N(t)} w_i \left[(T_1 - t_{\text{ref}})_i(t) - (T_2 - t_{\text{ref}})_i(t) \right] , \tag{41.7}$$

where $(T_x - t_{\text{ref}})_i(t)$ is the solution found in the CGGTTS file from station x for the satellite i at the epoch t, w_i is the weight, generally the $\sin^2(E)$ with E the satellite elevation, and $N(t)$ is the number of satellites simultaneously visible by the two stations. However, the quality of the CV solutions tends to degrade with increasing distance between the stations, since the number of simultaneously observed satellites decreases as the baseline increases.

An alternative to the common-view technique is therefore called the *all-in-view* (AV) approach: a clock solution $(T_x - t_{\text{ref}})(t)$ is computed independently for each station using all visible satellites and the difference is then computed afterward

$$(T_1 - T_2)(t) = \frac{1}{L(t)} \sum_{i=1}^{L(t)} w_{i1}(t)(T_1 - t_{\text{ref}})_i(t) - \frac{1}{M(t)} \sum_{i=1}^{M(t)} w_{i2}(t)(T_2 - t_{\text{ref}})_i(t) , \tag{41.8}$$

where $L(t)$ and $M(t)$ are the total number of observed satellites by stations 1 and 2, respectively, at the epoch t as in (41.7). AV is therefore independent of the distance between the stations. This is the same principle as precise point positioning (Sect. 41.2.4) but using only code measurements and fixing the position to its known value. Of course, the errors from satellite clock or ephemeris estimate do not cancel as they do in the common-view technique. Therefore, the use of precise ephemerides and clocks rather than the broadcast navi-

gation messages is mandatory [41.16]. Using IGS rapid products, the remaining uncertainties due to satellite orbits and clocks average appropriately to well below 100 ps for averaging 1 d and longer [41.17]. These authors also demonstrate the superiority of AV with respect to CV for baselines longer than 2000 km.

The choice between the CV and the AV will therefore rely on the distance between the stations where the clocks are located, and also the availability of precise orbits and clocks. CV will be preferred when only the broadcast ephemerides are available, but this approach should be restricted to short distance clock comparisons.

As the time transfer based on CGGTTS is a code-only analysis, both AV and CV are significantly affected by multipath of the code signals as well as uncertainties of the hardware delays. Depending on the station setup, some important diurnal variations can appear in the time transfer solution, which are not a clock variation but only the signature of the code multipath in one or both stations. An example is provided in Fig. 41.6, where specific patterns appear in the clock solution with a 23 h 56 min periodicity, that is, the needed time to retrieve the same geometrical relationship between the satellite, the receiving antenna, and the nearby reflectors.

To date, all in view time transfer using the ionosphere-free combination of GPS L1/L2 P(Y)-code observations constitutes the state of the art in GNSS time transfer using code measurements only. The statistical uncertainty (u_A) is at the level of a few nanoseconds, being limited by the current noise and multipath of the code measurements. The systematic uncertainty (u_B) relies on the calibration capabilities described in Sect. 41.3.2.

41.2.4 Precise Point Positioning

The noise and multipath of the code measurements in a code-only analysis masks the short-term stability of some atomic clocks, for example, hydrogen masers. A significantly higher stability can be obtained by using the carrier-phase measurements in addition to the code data. This requires a combined analysis of both code and carrier-phase measurements with a consistent modeling of these measurements similar to GNSS data analysis dedicated to precise positioning.

Only processing zero differences (e.g., precise point positioning) or single differences can be used for time transfer because the receiver clock disappears in double differences. Single differences rely on the same principle as the code-only CV approach, but using both code and carrier-phase measurements, while precise point positioning (PPP) relies on the same principle as the AV. As in the choice between CV and AV, PPP is usually preferred to single-difference analysis as independent on the baseline length. The impact of the satellite geometry on the single-difference solution was clearly demonstrated, for example, in [41.18], where differences between single-difference and PPP analyses reach the nanosecond level for an intercontinental baseline.

As explained in Chap. 25, PPP provides, besides the station position (static or kinematic), the tropospheric delay and the receiver clock solution. When used for time and frequency transfer, the station is of course considered as static, while the receiver clock is solved for each observation epoch. The receiver clock solution is, as explained before, $(t_{rec} - t_{ref})$ where t_{ref} is the reference time scale of the satellite clock products used in the PPP processing. The time transfer solution, as explained in Sect. 41.2, is then a difference between the clock solutions obtained for two remote stations.

It is mandatory that both PPP clock solutions have been computed using the same satellite orbit and clock products so that the reference is the same for both. Note that the IGS also provides receiver clock solutions $(t_{rec} - t_{ref})$ for part of the stations in the network. These are computed using zero differences, but the satellite and station clocks are computed at the same time, fixing the tropospheric delays to the values determined from a double difference network processing. As the IGS solution is based on the combination of solutions obtained by different analysis centers, it is usually considered as

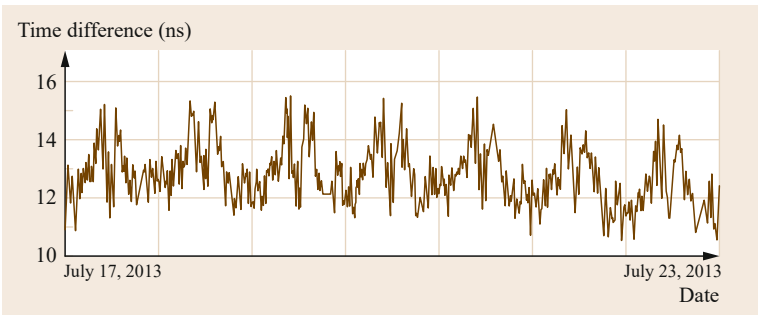

Fig. 41.6 Example of multipath impact in GNSS time transfer based on CGGTTS: clock comparison between the time laboratory ROA (Spain) and PTB (Germany), computed with the all in view technique based on the ionosphere-free combination of GPS P(Y)-code measurements on the L1 and L2 frequencies

the best solution available for the stations included in the network. The reference time scale of these solutions is the IGS time scale IGST (resp. IGRT) for the final (resp. rapid) products.

In a time transfer solution, the shape of the curve corresponds to the frequency variations between the two clocks (or timescales) compared, while the position of the curve on the *y*-axis corresponds to the time synchronization difference between the two clocks (or timescales). When the solution is computed using a combined analysis of code and carrier-phase measurements, the shape of the curve will be given by the carrier-phase data, while its position on the *y*-axis will be given by the code measurements. The carrier-phase data indeed contain an ambiguity term, which would put the solution on an arbitrary value on the *y*-axis. This ambiguity is determined for each satellite continuous track from the differences between the code and the carrier-phase measurements, and the final solution is then given by the carrier-phase data corrected for their ambiguity term. Thanks to their higher precision, carrier-phase data improve significantly the comparison of remote clock frequencies with respect to a code-only solution.

This improvement is illustrated in Fig. 41.7 for the comparison of two masers located in Brussels (Royal Observatory of Belgium) and Braunschweig (Physikalisch-Technische Bundesanstalt); both AV and PPP solutions are presented as well as their frequency

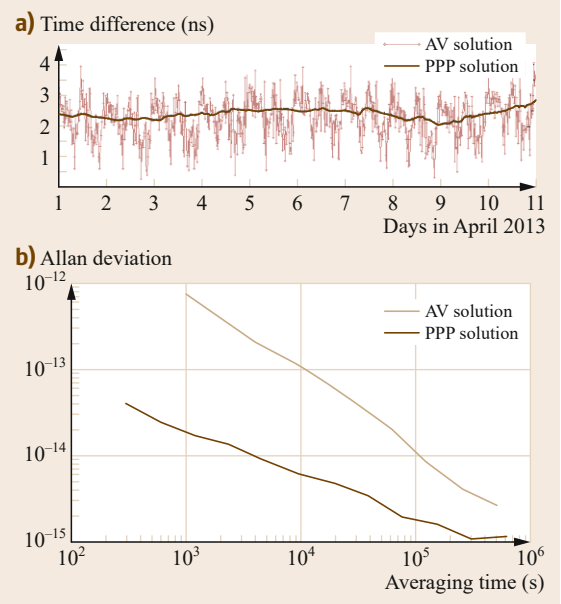

Fig. 41.7a,b Comparison of the time transfer solutions between two H-masers located in Brussels, Belgium and Braunschweig, Germany, computed with either AV or PPP **(a)** and associated Allan deviations **(b)**

stabilities highlighted by the Allan deviation. The statistical uncertainty u_A of PPP time transfer is currently below 100 ps for each observation epoch, allowing frequency transfer with an uncertainty approaching $1 \cdot 10^{-15}$ or even better for averaging times of one day [41.19–21]. The systematic uncertainty u_B of PPP time transfer is however the same as for code-only solutions, that is, a few nanoseconds, and relies on the calibration capabilities detailed in Sect. 41.3.2.

In a PPP analysis, the noise of the code measurements is responsible for jumps between successive and independent clock solutions. Indeed, as explained here above, the carrier-phase ambiguities are determined as the average over the continuous satellite track of the differences between the carrier-phase and code pseudoranges (maybe corrected with some bias to assure the integer nature of the ambiguity). As a consequence, the absolute values of the final PPP solution, that is, position of the curve on the *y*-axis, correspond roughly to the average of the code measurements of the data batch analyzed. Due to the noise of the code measurements, the standard error of the mean (SEM) is not zero and one can have jumps between two successive clock solutions. Consider, for example, one day of data sampled at 5 min with four visible satellites at each epoch. For a pseudorange pure white noise with an standard deviation of 30 cm, the standard error of the mean clock solution is then typically about 33 ps. This implies jumps between the successive daily clock solutions, distributed as a white noise with a zero mean and a standard deviation of 47 ps. However, the magnitude of these day-boundary jumps can be significantly larger [41.22]. The standard deviations of the jumps are station dependent, ranging from 150–1000 ps [41.23], well larger than the expected 47 ps. Only stations equipped with H-masers are considered there as for less stable frequency standards the clock instability dominates the day-boundary jumps caused by the pseudorange noise.

The origin of these large day-boundary jumps and of their station-dependent behavior is not yet fully understood, but reflects different station code performances, and reveals the colored signature of the code measurements. Several causes have already been identified, for example, a correlation with external temperature variations, but with opposite sign for different stations [41.22]. A large part of the day-boundary jumps (especially those of large magnitude) was also shown to be associated with pseudorange variations similar to all the satellites [41.24], with magnitudes reaching several nanoseconds, and possibly caused by instrumental delay variations (which can be due to temperature variations), reflections in the cable connectors or some nongeometrical near-field effect.

As an example, Fig. 41.8 presents the PPP clock solution for the IGS station OPMT (Paris) equipped with a H-maser. Based on the use of IGS final products, the solution corresponds to (OPMT-IGST). A same linear term was removed from all the curves in order to facilitate the visibility. The results depicted in Fig. 41.8 correspond to (1) a PPP solution from daily processing, (2) a PPP solution from a unique process of a one month data batch (computed by the BIPM for the computation of UTC), and (gray dots) a code-only solution plotted for each satellite separately. The observed day boundary jumps in curve (1) are because the absolute value of the PPP solution corresponds to the average of the code measurements of the data batch analyzed, while these code measurements suffer from some long-term variations, as seen from the code-only solution (gray dots). For comparison, the PPP solution computed for the complete five day data batch is of course continuous across the day boundaries. Note that the two PPP solutions presented in Fig. 41.8 have been produced by two different software tools, which explains the small differences in the subdiurnal variations.

Several approaches have been addressed in order to reduce or eliminate the daily discontinuities. Correcting the jumps observed in the clock solution when the ambiguities are still float in the solution produces a random walk of the continuous solution [41.20]. Processing multiday data batches [41.25] as proposed in curve (2) of Fig. 41.8, transports of course the problem at the batch boundaries, but in that case the jumps are smaller as the impact of the code noise is reduced thanks to the increased number of observations. A dedicated data filtering method [41.26] was also proposed, as well as processing sliding windows [41.27] but again the problem is mitigated rather than solved.

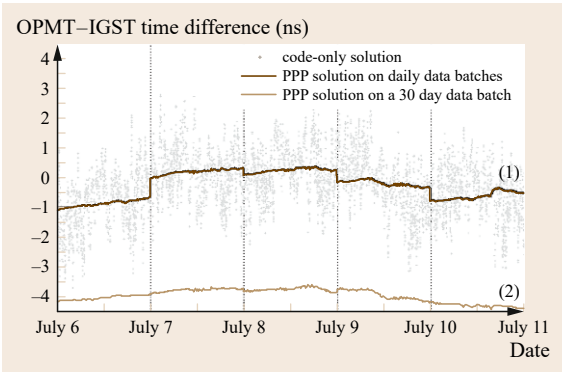

Fig. 41.8 PPP solutions for the station OPMT (Paris) equipped with a H-maser. Solution *(1)* is based on daily process, while solution *(2)* was obtained from the analysis of a one month data batch. *Gray dots* are the code-only solutions plotted for each satellite separately. In order to improve the visibility, a same linear term was removed from all the curves as well as a 3 ns bias from curve *(2)*

The optimal way to produce independent solutions while ensuring their continuity is to fix the ambiguities to integer values [41.28]. This requires the introduction of some station and satellite biases to absorb the non integer part of the ambiguities. In the results produced by this integer PPP processing, the day boundary discontinuities still exist but are always an integer number of cycles of the narrow-lane combination of the two frequencies used in the ionosphere-free combination; these integer jumps can then be easily canceled out [41.29]. Equivalently, in [41.30] a new parametrization is proposed that separates the pseudorange observation colored noise from the carrier-phase parameters, that is, ambiguities and clock; the continuity is then directly obtained between independent PPP solutions of successive data batches, but requires to arbitrarily fix one initial receiver bias.

All these issues related to the continuity of the PPP solutions at the batch boundaries and to the reduction of the impact of the noisy code measurements find their importance in the wish to improve the performances of GNSS frequency transfer. The time transfer quality however always relies on the code measurements, and the best way to improve these measurements will be to design an antenna setup which reduces the near-field multipath. Using either absorbing material around the antenna or a pillar of at least 2 m height supporting the antenna, have for example, shown convincing results in reducing the magnitude of the day boundary jumps [41.31], or [41.32]. Furthermore, antenna cables with low sensitivity to temperature variations, and a stabilized temperature around the clock and receiver are as well recommended to reduce pseudorange coloured noise.

A last point to be emphasized is the correlation between the clock and the tropospheric zenith path delay (TZD) estimated in the PPP processing. It was, for example, demonstrated that a short sampling rate (shorter or equal to 15 min) in the estimation of the TZD is mandatory to reproduce as much as possible the true troposphere variations and hence to avoid any contamination of the clock solution from unmodeled short-term tropospheric changes [41.33]. The details of the mapping function employed have however no significant impact [41.34].

The ultimate performances of GNSS frequency transfer can be estimated using a pair of stations in a common-clock setup, that is, both connected to a same clock, so that the solution is not influenced by the clock instability. The Allan deviation of such solutions

are presented in Fig. 41.9. The common-clock results were obtained using two separate receiving chains with a distance of 100 m between the antennas. In order to emphasize the impact of the code measurements on the stability of the solutions, Fig. 41.9 presents, for this common-clock setup, one classical PPP solution and one solution obtained using only carrier-phase data. In latter, the single differences of carrier-phase data were used and the ambiguities were determined with respect to zero (the expected clock difference) rather than with respect to the code single differences as is the case in PPP. Therefore, only the noise of the carrier-phase data influences the solution. Note that for nearby stations, processing single differences or PPP provides similar results as PPP because of the geometry of satellites which is exactly the same for both stations. The impact of any error on satellite products has therefore exactly the same impact on the PPP solutions of both stations, and cancels out in the difference of the PPP solutions while in single differences it cancels out at the level of observations. The second curve results from a PPP analysis using the NRCAN PPP software on a multi-day basis [41.25] in order to avoid a contamination of the Allan deviation from the day-to-day discontinuities inherent to daily processing of PPP. The difference between these two curves comes by using code measurements in the PPP case, which degrades the stability at intervals of a few hours, that is, the classical duration of the satellite visibility on which the ambiguities are constant.

The two other curves of Fig. 41.9 present the Allan deviation of the PPP solutions for the links Brussels–Washington (BRUS-USN3, about 6000 km) and Brussels–Paris (BRUX-OPMT, about 300 km). Both provide approximately the same quality. The short-term stability is however lower than what was expected from the common-clock results; the origin of this degraded quality has not yet been identified to date. The H-maser stability curve in the figure shows that H-maser instabilities dominate over periods longer than 3 h, so that the curves (3) and (4) associated with H-maser comparisons cannot provide information about the performance of the technique; only the common-clock setup can be used to this end. The optical clock stability curves show that optical clock comparisons from GNSS will be possible only for averaging times longer than several days.

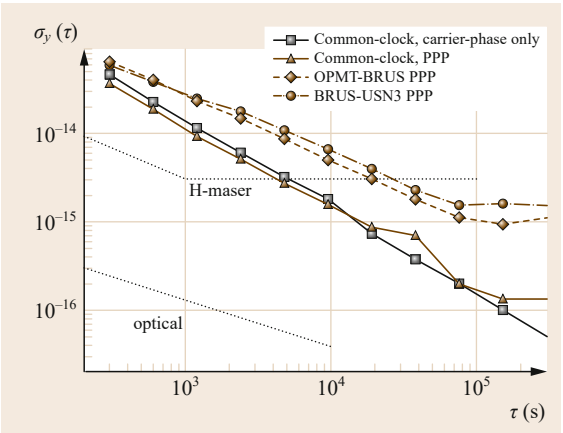

Fig. 41.9 Allan deviation of the clock solutions estimated with state-of-the-art GNSS frequency transfer compared with the Allan deviation of the most stable atomic clocks to date, that is, the H-masers and optical frequency standards. The clock solutions correspond to two links among stations equipped with H-masers: Brussels–Paris (BRUS-OPMT, 300 km), Brussels–Washington (BRUS-USN3, 6000 km); the 100 m baseline is using the same clock for both stations so that the solution does not depend on the stability of the clock and shows the maximum capabilities of the method

41.3 Hardware Architecture and Calibration

The GNSS equipment needed for time and frequency transfer consists of a receiving antenna connected via cable to a dedicated GNSS receiver and some cable link between the receiver and the external clock to be examined. For time transfer, it is also necessary to have access to the 1 pps given by the external clock, and each of the just mentioned components should be calibrated, which means that the hardware delay of each signal in these instruments or cables should be accurately determined. This section describes the characteristics of dedicated GNSS receivers for time/frequency transfer, and the existing methods for calibrating the receiving chain.

41.3.1 Time Receivers

Specific GNSS receivers have been developed and commercialized for time transfer. The receiver system consists of an input for an external frequency reference (typically 5 or 10 MHz) to be used in all internal oscillator functions, an input for an external pulsed signal related to the external clock 1 pps, and possibly an in-

ternal time-interval counter. The components may be integrated into a single package or may be separate and connected together by appropriate cables.

Figure 41.10 shows three types of receivers satisfying these requirements. The epoch of the receiver clock can be either:

- Based on the GNSS signals themselves and continuously monitored against the 1 pps signal of the external clock using a time-interval counter (R1 and R2).
- Locked directly to the 1 pps signal from the external clock (R3).

The classical geodetic receiver (R1) can be used for time transfer only if the 1 pps output is related to the internal reference (or receiver clock), and if the relation between the internal reference and the 1 pps output is perfectly known: it must be provided by the manufacturer or measured by the user following a given procedure which is different for each receiver make. The time interval counter (TIC) for R1 and R2 measures the synchronization error between the receiver internal clock and the external clock to be examined. This TIC should measure time intervals (of up to 1 s if required) with a u_B uncertainty approaching 100 ps or better, and a noise level below 100 ps; the TIC measurements should furthermore be reported separately from the GNSS measurements. The main difference between the receiver types R1 and R2 is that the TIC and the computation of the CGGTTS data are inside the receivers R2 while they are external to the classical geodetic receivers R1; for these receivers, the CGGTTS files will be generated using an external software tool that combines the raw measurements available in, for example, Receiver INdependent EXchange format (RINEX (Annex A.1.2) files and the TIC measurements.

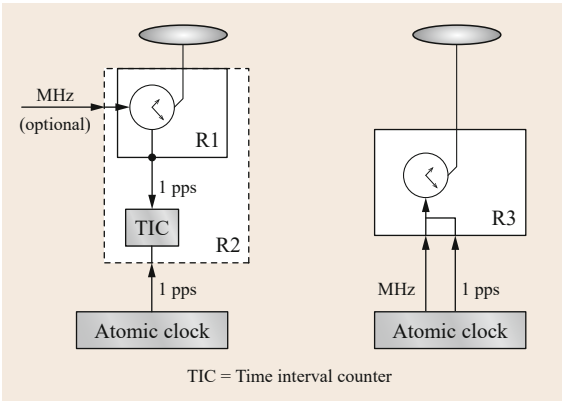

Fig. 41.10 Different kinds of receiver setups for GNSS time and frequency transfer. R1 and R2 use their own internal clock and compares it with the external clock using a time interval counter, while R3 directly uses the 1 pps of the external clock as internal reference

In order to overcome the possible noise introduced by the TIC, some geodetic + time receivers (R3) directly synchronize their internal clock (modulo one constant bias) on the external clock to be compared. The user must in that case ensure that the 1 pps signal is coherent with the frequency reference and maintained sufficiently close to the GNSS time scale to assure proper operation. The input 1 pps allows the receiver to choose without ambiguity one particular cycle of the input frequency to form its internal time reference. The receiver clock is so locked in phase on some given point of the input frequency following the pulse of the input 1 pps signal. This kind of receiver cancels the need for a time interval counter and hence provides a final clock solution which is less noisy than the solutions obtained with R1 or R2. Furthermore, the CGGTTS results can be obtained directly from raw measurements available in the RINEX files, using a dedicated software tool as proposed, for example, in [41.35]. In receiver type R3, the internal reference is obtained either by locking the internal oscillator on the external frequency, or by using directly the external frequency for the internal reference. If the internal oscillator is locked on the external frequency with an enslavement system, then the system must be described in full details by the manufacturer to allow for accurate calibration (Sect. 41.3.2). This system must furthermore be designed to introduce no noise on the frequency; adding noise would make impossible the study of frequency stabilities of the best frequency standards via GNSS frequency transfer. Furthermore, the way the internal reference clock is obtained from the external 1 pps must also be described by the manufacturer; this is mandatory to have access to the delay between the external clock and the GNSS measurements, and hence to correctly transfer time.

The Consultative Committee for Time and Frequency (CCTF) advocated in its recommendation S5(2001) [41.36] that the manufacturers of receivers used for timing with GNSS implement the technical guidelines for receiver hardware compiled by the CCTF group on GNSS time transfer standards (CGGTTS). These guidelines have been compiled with the aim of achieving a system that can transfer time with an accuracy of 1 ns or better. A detailed review and extension to new systems can be found in [41.37].

41.3.2 Hardware Calibration

As already stated, GNSS measurements can be exploited for time transfer only if the electric delay accumulated by the signal between the antenna phase

center and the internal timing reference of the receiver is accurately known, as well as the synchronization error between this internal timing reference and the external clock to be examined. Note that the satellite hardware delay being the same for all the ground observing stations, it is already included in the satellite clock and need not be corrected for in the GNSS analysis dedicated to time transfer. One exception comes however when the code measured by the receiver are not the same as the codes used for the satellite clock determination. This happens, for example, when the receiver measures the GPS L1 C/A code. All the clock products for GPS satellites are indeed based on the ionosphere-free combination of L1/L2 P(Y)-codes. Using the combination of L1 C/A and L2 P(Y) code measurements requires therefore a transformation of the satellite clock products to the same combination, using the satellite differential code biases L1 C/A–L2 P(Y) that are provided, for example, by the IGS (Sects. 19.6.1 and 21.3.1).

The station hardware delays, in contrary, must be determined by calibration, as well as the exact time offset between the receiver internal clock and the external clock. All these delays are represented schematically in Fig. 41.11 for the three types of receivers described earlier.

Hardware delays exist in both code and carrier-phase measurements. However, only the code delays are determined by calibration and corrected for in time transfer computation, since only the code measurements provide the time. When carrier-phase data are used, the phase delays are absorbed in the ambiguities.

The first category of delays consists of the electric delays affecting the GNSS signals, that is, δ_A the antenna delay, δ_{AC} the antenna cable delay, and δ_R the receiver delay, that is, between the antenna cable

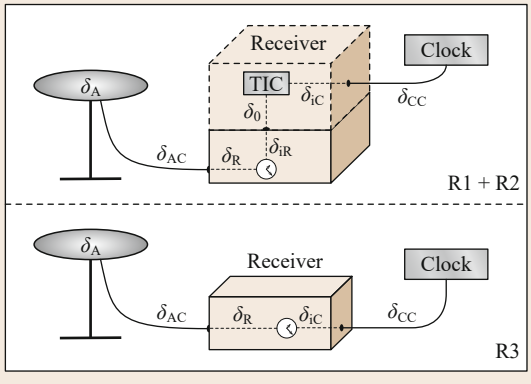

Fig. 41.11 Hardware delays to be accounted for time transfer and associated with three types of receivers of Fig. 41.10

connector and the internal reference where the measurement is made. These instrumental delays are present in the term errors of (41.4) When extracting them explicitly one gets

$$P = \|\boldsymbol{x}_s - \boldsymbol{x}_r\| + c(\Delta t_{rec} - \Delta t_{sat}) + B(\text{rec}) + \epsilon \,, \quad (41.9)$$

where B(rec) is the bias associated with the signal delay accross the antenna, the antenna cable, and the receiver

$$B(\text{rec}) = \delta_A + \delta_{AC} + \delta_R \,. \quad (41.10)$$

This bias should therefore be removed from the code measurements to retrieve the accurate synchronization error $(t_{rec} - t_{ref})$ between the receiver clock and the reference time scale. B(rec) should be constant. It is however sensitive to temperature variations, so that a temperature stabilization is recommended in the receiver room, as well as choosing an antenna cable with low sensitivity to temperature variations.

The second category of delays consists of the synchronization error between the internal timing reference and the external clock to be examined. For receivers with an internal or external time interval counter (i. e., R1 and R2), the synchronization error is measured by the TIC. This measurement must however be corrected for:

- The delays in the cables and electronic devices transporting the 1 pps signal from the clock to the TIC, that is, $(\delta_{iC} + \delta_{CC})$ for receivers R1 or δ_{CC} for receivers R2.
- The delays in the cables and electronic devices transporting the 1 pps signal from the receiver clock to the TIC, that is, δ_0.
- The synchronization error between the internal reference and the 1 pps output of the receiver, that is, δ_{iR}, to be provided by the manufacturer.

When the receiver clock is directly using the frequency and time signals from the external clock (i. e., R3), only the clock cable delay δ_{CC} should be measured, and added to the bias δ_{iR} provided by the manufacturer. This second category of delay has to be added from the GNSS solution to go back from the receiver clock to the external clock.

Finally the synchronization error between the clock and the reference of the satellite clock products is for R1 and R2

$$\begin{aligned}(T - t_{ref}) = {} & (t_{rec} - t_{ref})_{PR} \\ & - (\delta_A + \delta_{AC} + \delta_R) \\ & + \text{TIC} + \delta_{CC} + \delta_{iC} - \delta_{iR} - \delta_0 \,, \end{aligned} \quad (41.11)$$

while for the receiver R3 it reads

$$(T - t_{\text{ref}}) = (t_{\text{rec}} - t_{\text{ref}})_{\text{PR}} - (\delta_{\text{A}} + \delta_{\text{AC}} + \delta_{\text{R}}) + (\delta_{\text{CC}} + \delta_{\text{IC}}) \,, \tag{41.12}$$

where $(\ldots)_{\text{PR}}$ denotes the time offset as derived from pseudorange measurements.

The cable delays are independent of the signal frequency, and correspond to the product between the cable length and the group velocity of the signal in the cable given by

$$v_{\text{g}} = \frac{c}{\sqrt{\varepsilon_{\text{r}}}} \,, \tag{41.13}$$

where v_{g} is the group velocity, c the velocity of light and ε_{r} the relative dielectric permittivity (Sect. 6.1). The connectors at both ends of the cable also induce some delays that must be taken into account. The group delay in the cable with its connectors can be measured with an accuracy of some tens of picoseconds using a time interval counter or a vector network analyzer (VNA). The offset δ_{IC} can only be determined if either the receiver offers an access to its internal clock via, for example, a 1 pps output synchronized on the internal clock, or the receiver manufacturer provides a detailed explanation of how the internal clock is constructed from the combination of input 1 pps and frequency coming from the external clock, so that it can be reproduced to be measured outside the receiver.

The antenna and receiver delays affecting the GNSS signals (δ_{A} and δ_{R}) are both frequency dependent. Two techniques exist to date for their calibration: the relative technique, using true GNSS signals, and the absolute technique using simulated GNSS signals. Note that the antenna calibration concerned here differs from the one discussed in 17.6.2 of this Handbook, which aims at determining the accurate phase center, while in the present case it determines the electric delay of the signal in the antenna. Neither elevation nor azimuth dependence of this delay is considered to date.

Absolute Calibration

The principle of the absolute calibration is to use simulated signals in order to determine the electric delay of the receiver or antenna (or the complete receiving chain), and compare the receiver/antenna measurements to the simulated signals. Complete descriptions of the method can be found, for example, in [41.38–40] and references therein. The simulated signal is produced by a GNSS signal generator, and is free of noise or perturbation like atmospheric delays or multipath existing in the case of true GNSS signals. This kind of calibration offers a very high accuracy of 0.4 ns [41.41] while it requires the use of a GNSS simulator and a VNA, as well as an anechoic chamber for the antenna, which are not existing in the major part of the laboratories. Moreover, this method does not allow one to determine the hardware delays of already operational receiving chains, as these may not be interrupted and the antenna is calibrated in nonreal conditions.

Relative Calibration

Much more simple to be technically implemented is the relative calibration technique, which is consequently used for all operational stations. It consists in a comparison of pseudorange measurements collected by the local receiving chain and a reference receiving chain traveling from laboratory to laboratory [41.42]. For this, both stations should be connected to the same clock and installed in co-location (Fig. 41.12), so that all the perturbations except the multipath are equal. The difference of the pseudoranges measured by the two receiving chains then contain only a difference in antenna position plus the differences between the hardware delays of the two stations. Using the same nomenclature as in Fig. 41.11, this gives for a given satellite s and a given code c

$$\begin{aligned} P_{\text{lab}}(c,s) - P_{\text{ref}}(c,s) &= \|\boldsymbol{x}_s - \boldsymbol{x}_{\text{lab}}\| - \|\boldsymbol{x}_s - \boldsymbol{x}_{\text{ref}}\| \\ &\quad + (\delta R + \delta A)_{\text{lab}} - (\delta R + \delta A)_{\text{ref}} \\ &\quad + (\delta_{\text{AC}} - \delta_{\text{CC}} - \delta_{\text{IC}})_{\text{lab}} \\ &\quad - (\delta_{\text{AC}} - \delta_{\text{CC}} - \delta_{\text{IC}})_{\text{ref}} + \epsilon \,, \end{aligned} \tag{41.14}$$

where ϵ is the combined noise and multipath of the two stations. The terms $(\delta_{\text{AC}} - \delta_{\text{CC}} - \delta_{\text{IC}})$ can be measured and deduced from the receiver manufacturer information for both receivers. The difference of pseudoranges therefore provides the $(\delta R + \delta A)$ of the laboratory receiver chain with respect to the reference chain. If this reference chain has been absolutely calibrated, the relative calibration then gives access to the true hardware

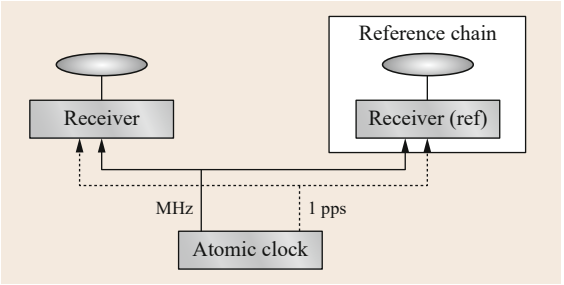

Fig. 41.12 Setup for relative calibration exercise

delay of the laboratory receiver+antenna. If not, then the relative calibration data can be used to calibrate a time transfer link in which the same reference chain was used for the calibration of both stations. In that case [41.43], the reference station has to be installed in co-location with the two stations of the link, and the calibration exercise provides the quantity $(\delta R+\delta A)_1-(\delta R+\delta A)_2$ which can be directly applied to the time transfer solution T_1-T_2. The same strategy can be applied to a network of stations in which all the stations are differentially calibrated with respect to a same reference. Any time link of the network will then be correctly calibrated by applying the computed relative hardware delays $(\delta R+\delta A)$ to each of the stations.

The relative calibration technique just described does not allow separating the hardware delays of the antenna and of the receiver. The isolated effect of receiver and antenna could be determined connecting the two receivers to the same antenna, using a splitter. However, the hardware delays of GNSS signals in the splitter are really difficult to be measured, and the splitter introduces a source of signal reflections, also called cable multipath, possibly inducing interferences [41.44]. Solutions to overcome that problem exist [41.40] but require the use of amplifiers and attenuators of which the levels have to be chosen thoroughly as a function of the antenna and receiver types. It is therefore recommended to use relative calibration only for the determination of the combined receiver plus antenna hardware delays.

The uncertainty budget of the differential calibration technique gives 2.3 ns for each isolated code [41.45], when taking into account the uncertainty on the absolute calibration of the reference chain, on the cable delay measurements, and the noise of the code measurements. In parallel, the uncertainty on the difference between two codes (e.g., L1/L2 P(Y) for GPS) is estimated to 2.0 ns so that the associated uncertainty on the ionosphere-free combination is 3.8 ns. Considering a time transfer between two stations independently calibrated provides a type B uncertainty on the link at the level of 5.4 ns reduced to 5 ns in BIPM circular T. However, this 5 ns uncertainty reflects the long-lasting conservative practice. A significantly reduced uncertainty was found in [41.43] using a traveling receiver. The technique was then refined to reach an uncertainty around 1 ns in [41.46] and [41.47]. Such small u_B value however can be maintained over long times only if periodic re-calibrations are made.

The challenge for relative calibration is furthermore to keep constant the hardware delays of the reference station. The reference equipment is always subject to possible damages or instabilities due to its traveling between stations. The local temperature and humidity conditions in different locations can furthermore be very different from the conditions during the absolute (or relative) calibration of the reference equipment, which can cause some biases in the results [41.48]. While receivers can be installed in temperature-controlled rooms, the antenna and antenna cables can suffer diurnal temperature changes of around 40 °C, as occur in certain parts of the world. Some experiments of measuring the temperature sensitivities of the antennas showed maximum diurnal variations (for diurnal variations of 20 °C) of 40 ps for the carrier-phases [41.49], while up to 2 ns for the code measurements [41.50, 51]. Special attention should therefore be paid to sensitivity to temperature variations for the choice of the antenna and cable of the traveling reference GNSS station, as well as any other GNSS station dedicated to time transfer. The stability of the reference GNSS station should furthermore be regularly verified, by intercomparison with fixed stations. The delays of the most stable GPS common-view time transfer receivers vary typically by a few nanoseconds over years, generally by less than 5 ns peak-to-peak [41.52].

41.4 Multi-GNSS Time Transfer

41.4.1 General Requirements

The combination of measurements from different GNSS constellations for time transfer requires several specifications. The first one is that the receiver internal reference be the same for all systems. A second requirement is that the receiver must be fully calibrated, that is, the hardware delays must be determined for each signal transmitted by each constellation. Indeed, in some cases the frequency bands used by different systems do not completely overlap, or the power spectrum inside the band is not the same. For example in GLONASS, several carrier frequencies are used in each frequency bands (Chap. 8), yielding complex calibration procedures due to the need to calibrate one delay per carrier frequency.

Finally, a last requirement concerns the reference of the satellite clock products. The receiver clock solution obtained from observations of satellites belonging to constellations A and B are $(t_{rec}-t_{ref,A})$ and $(t_{rec}-t_{ref,B})$, where $t_{ref,A}$ and $t_{ref,B}$ are the reference time scales of the two constellations. In order to get only one combined

receiver clock solution, the user should either know the accurate de-synchronization $(t_{\mathrm{ref,A}} - t_{\mathrm{ref,B}})$ at each observation epoch, or use satellite clock products having the same reference whatever the constellation to which they belong, or introduce $(t_{\mathrm{ref,A}} - t_{\mathrm{ref,B}})$ as unknown and then estimate it along with the other parameters. As $(t_{\mathrm{ref,A}} - t_{\mathrm{ref,B}})$ is generally not available at each observation epoch, only the two other possibilities can be used. The last one however requires the estimation of one additional parameter at each observation epoch which increases the uncertainty of the solution. The optimal option is therefore the second one. Combined products already exist for GPS and GLONASS satellites, they are provided by some analysis centers of the IGS. It is assumed that in the future, such products will also be provided for Galileo and BeiDou. The combination of all these constellations in one global time transfer solution will therefore be possible with the second option. We describe here the case of GLONASS which requires a special treatment due to existence of interfrequency biases, and present some first results on the use of Galileo and BeiDou for time and frequency transfer. Note that QZSS can also be used for regional clock comparisons, while it will play no role in intercontinental time transfer.

41.4.2 GPS + GLONASS Combination

The main difference between GLONASS and the other GNSS is the channel access method. While all the GNSS constellations use the code division multiplex access (CDMA) technique in which all the satellites share the same carrier frequencies, GLONASS is based on the frequency division multiple access (FDMA) technique. Each GLONASS satellite transmits consequently on a different frequency in the L1 band as well as in the L2 band.

Due to the frequency-dependent nature of the hardware delays in the receiver and in the antenna, these are different for each GLONASS satellite group transmitting a given pair of frequencies L1, L2, inducing interfrequency biases up to tens of nanosecond in the code measurements and hence in the clock solutions as determined from different satellites. The observation equation (41.9) should therefore be modified for GLONASS satellites as

$$P = \|\boldsymbol{x}_{\mathrm{s}} - \boldsymbol{x}_{\mathrm{r}}\| + c(\Delta t_{\mathrm{rec}} - \Delta t_{\mathrm{sat}}) + B(\mathrm{rec,sat}) + \epsilon \ . \quad (41.15)$$

In this case, the bias B(rec,sat) being satellite dependent cannot be absorbed by the receiver clock Δt_{rec}. Note that, in principle, bias should be the same for satellites using the same frequency pair, but it is rarely modeled as such, and a satellite-dependent bias is generally preferred.

The satellite clock Δt_{sat}, the receiver clock Δt_{rec}, and the bias B(rec,sat) in equation (41.15) cannot be separated unequivocally. As a consequence, the GLONASS satellite clocks determined from some network analysis are affected by artificial biases. In that computation, it is indeed necessary to fix arbitrarily one bias for a given receiver–satellite pair and then to determine all satellite clocks, receiver clocks and receiver–satellite biases with respect to that fixed parameter. If the fixed bias changes between the treatments of two successive data batches, the biases for all station–satellite pairs will change accordingly. As classically the satellite clock products are computed on a daily basis, their use to determine the clock solution of a single station (in AV or PPP) requires the estimation of daily receiver–satellite biases $B'(\mathrm{rec, sat, day})$ in addition to the clock solution. These biases contain a physical part, corresponding to the station hardware delays for the frequency emitted by the satellite, and which is constant (or nearly constant) over the long-term, plus an artificial bias present in the satellite clock products

$$B'(\mathrm{rec, sat, day}) = B(\mathrm{rec,sat}) + \gamma(\mathrm{sat, day}) \ , \quad (41.16)$$

B(rec,sat) corresponds to the terms $(\delta_{\mathrm{A}} + \delta_{\mathrm{AC}} + \delta_{\mathrm{R}})$ in (41.11), that is, the sum of antenna delay, antenna cable delay and receiver delay.

As the biases $\gamma(\mathrm{sat, day})$ are the same for all the GNSS stations, they cancel out in the common view approach (Sect. 41.2.3) and a calibrated GLONASS clock solution can be obtained if B(rec,sat) is known for both stations of the link, that is, if the stations have been calibrated for all the GLONASS frequencies.

However, such a calibrated clock solution cannot be obtained with the PPP and AV techniques using only GLONASS measurements due to the unknown biases $\gamma(\mathrm{sat, day})$. The combination of GPS plus GLONASS measurements allows one to solve for that issue. Two approaches are then possible: the first one uses only the GPS calibration results and determines the biases $B'(\mathrm{rec, sat, day})$ as the differences for each satellite and each day, between the noncalibrated GLONASS clock results and the calibrated GPS clock solution.

An application of this technique for the computation of all in view solutions based on CGGTTS results was presented in [41.53], and the corresponding combination of GPS and GLONASS in precise point positioning can be found in [41.54]. However, in both cases the GLONASS measurements are not calibrated which is not convenient from the metrological point of view but is a consequence of the unknown bias present in the satellite clock products. The second possibility is to use

a link approach. The basic idea is that the differences between the estimated $B'(\text{rec}, \text{sat}, \text{day})$ for the two stations of the link reads

$$B'(\text{rec}_1, \text{sat}, \text{day}) - B'(\text{rec}_2, \text{sat}, \text{day}) = B(\text{rec}_1, \text{sat}) - B(\text{rec}_2, \text{sat}) \quad (41.17)$$

that is, does not depend any more on the biases of the satellite clock products, and can be accurately determined by a calibration exercise. The values of $B(\text{rec}_1, \text{sat}) - B(\text{rec}_2, \text{sat})$ can then be used to constrain the determination of $B'(\text{rec}_1, \text{sat}, \text{day})$ and $B'(\text{rec}_2, \text{sat}, \text{day})$. This requires, of course, that the clock solutions (AV or PPP solutions) of the two stations are determined in a same analysis procedure [41.55]. Finally, the clock solutions obtained from the combination of GLONASS and GPS measurements provide a same level of performances than the GPS-only solutions, as shown in the publications cited earlier.

41.4.3 Time Transfer with Galileo and BeiDou

As stated in Chap. 9, Galileo is transmitting in three frequency bands (E1, E5, and E6), but only the two former ones are available in the open service. Most dual-frequency receivers measure the unencrypted ranging codes E1 and E5a, and improved-accuracy receivers measure additionally the signal E5b and the wide-band E5 alternative binary offset carrier (AltBOC) signal.

Some first experiments of using the Galileo signals for time transfer were already realized, based on the ionosphere-free combinations of E1 with either E5a, or E5b or E5 AltBOC. The results indicate that the noise of the Galileo measurements is significantly lower than the noise of the ionosphere-free combination of the GPS measurements P(Y)-codes on L1 and L2 at all elevations [41.56]. This comes partly from the smaller coefficients multiplying the code measurements (and hence the noise) in the ionosphere-free combination. These coefficients are indeed smaller for more distant frequencies, as is for (L1, L5) with respect to (L1, L2). The noise of the final solution however depends of the number of visible satellites so that Galileo will compete with GPS only when the full constellation will be deployed.

First steps in BeiDou time transfer have also been started [41.57]. From theoretical point of view, the noise of the ionosphere-free combination should not be so much lower than the present GPS noise, due to the proximity of the frequencies of the open service (B1 and B2), but no rigorous comparison exists to date.

It must however be noted that as GPS, Galileo, and BeiDou are based on the CDMA technique, so that a same total hardware delay affects the code measurements from all the Galileo satellites, and a same corresponding hardware delay affects the code measurements from all the BeiDou satellites. No satellite-dependent hardware delay should be determined as is the case for GLONASS. The combination of GPS with Galileo and/or BeiDou will therefore increase the number of observations without increasing the number of unknowns (except in PPP where additional phase ambiguities will have to be resolved), and an improvement by a factor of $\sqrt{3}$ is expected from the combination of GPS with the full Galileo and BeiDou constellations.

41.5 Conclusions

This chapter presented the time and frequency applications offered by the GNSS, as well as their current performances summarized in Table 41.1. Accurate time or time transfer can be realized with an accuracy approaching one nanosecond thanks to most advanced calibration techniques. Due to the noise and multipath of the code pseudoranges, the accurate frequency transfer will be preferably determined with PPP which makes use of the carrier-phase measurements, and which allows comparing atomic clocks at the level of $1 \cdot 10^{-13}$ for short averaging times (some minutes) and approaching $1 \cdot 10^{-16}$ at one day averaging times. These ultimate performances can of course be reached only with appropriate instrumentation.

In the future, GNSS may grow to include more than 100 satellites, mostly in medium Earth orbit, with some in geostationary and inclined elliptical orbits. Using the

Table 41.1 Summary of the best performances of GNSS timing applications

Application	Parameter	Performance
Synchronization on UTC[a]	u_B u_A	20 ns 10 ns
Frequency steering (GNSSDO)[b]	Stability	$\leq 1 \cdot 10^{-12}$ one day
Time transfer with CGGTTS[c]	u_B u_A	< 2 ns 2 ns
Time transfer with PPP[c]	u_B u_A	< 2 ns 100 ps
Frequency transfer with PPP[b]	Stability	$2 \cdot 10^{-16}$ one day

[a] Function of the GNSS prediction of UTC and of the receiver calibration
[b] Given by the Allan deviation
[c] Function of the receiver calibration

same kind of signals from different constellations will increase the number of measurements in the averaging procedure, and hence produce a slight improvement in terms of precision [41.58]. Furthermore, each of the GNSSs will be gradually modernized with, for example, new onboard clocks for GPS, or transfer to the CDMA technique for GLONASS which will eliminate the inter-channel biases.

However, the added value of these constellations resides also in the new possibilities they offer thanks to new ranging signals having more complex structure and improved characteristics. We can, for example, expect new timing performances thanks to the precise Galileo E5 AltBOC signal, whose combined noise and multipath is limited to less than 25 cm at all satellite elevations [41.59]. If in the future, GNSSs offer some new signals in the C-band (or Ku band), the ionosphere-free combination with code measurements in the L-band would also mitigate the noise amplification due to the coefficients of the linear combination.

In parallel, some new clock comparison techniques will be offered by the GNSS for fundamental time metrology. BeiDou, for example, will provide, besides the timing services described in this chapter, a two-way time transfer, that is, based on signals that travel both ways between the two ground clocks to be compared via a BeiDou geostationnary satellite equipped with a transponder [41.60]. This technique is already widely used by the time laboratories for their participation to TAI [41.61] but relies presently on commercial satellites. BeiDou will be the first navigation system to propose that alternative to the classical one-way method. The station equipment for that technique will however be completely different from the classical GNSS receiving station, as an emission unit must be considered as well. BeiDou and GLONASS will additionally allow laser time transfer as the satellites are equipped with laser reflectors, offering to compare remote ground clocks with accuracy levels not achievable by radio systems. A first experiment with BeiDou demonstrated a precision of approximately 300 ps on the clock difference and relative frequency stability of $1 \cdot 10^{-14}$ for the comparison between a ground hydrogen maser and satellite rubidium clocks [41.62]. Finally, future generations of the GNSS, still under study, will open in the next decades still new horizons for time and frequency metrology.

References

41.1 H.-G. Berns, T.H. Burnett, R. Gran, R.J. Wilkes: GPS time synchronization in school-network cosmic ray detectors, IEEE Trans. Nucl. Sci. **51**(3), 848–853 (2004)

41.2 E. Butterline, J. Abate, G. Zampetti: Use of GPS to synchronize the AT&T national telecommunicaitons network, Proc. 21th Annu. PTTI Appl. Plan. Meet. (1988) pp. 65–75

41.3 I. Hall, P.G. Beaumont, P.G. Baber, I. Shuto, M. Saga, K. Okuno, H. Uo: New line current differential relay using GPS synchronization, Proc. IEEE Power Tech Conf., Bologna (2003) pp. 1–8

41.4 Joint Committee for Guides in Metrology: Evaluation of measurement data: Guide to the expression of uncertainty in measurement, JCGM 100:2008, http://www.bipm.org/utils/common/documents/jcgm/JCGM_100_2008_E.pdf (2008)

41.5 E.F. Arias: The metrology of time, Phil. Trans. R. Soc. A **363**, 2289–2305 (2005)

41.6 M. Lombardi: The use of GPS disciplined oscillators as primary frequency standards for calibration and metrology laboratories, Measure **3**(3), 56–65 (2008)

41.7 The OPERA Collaboration, T. Adam, N. Agafonova, A. Aleksandrov, O. Altinok, P. Alvarez Sanchez, A. Anokhina, S. Aoki, A. Ariga, T. Ariga, D. Autiero, A. Badertscher, A. Ben Dhahbi, A. Bertolin, C. Bozza, T. Brugière, R. Brugnera, F. Brunet, G. Brunetti, S. Buontempo, B. Carlus, F. Cavanna, A. Cazes, L. Chaussard, M. Chernyavsky, V. Chiarella, A. Chukanov, G. Colosimo, M. Crespi, N. D'Ambrosio, G. De Lellis, M. De Serio, Y. Déclais, P. del Amo Sanchez, F. Di Capua, A. Di Crescenzo, D. Di Ferdinando, N. Di Marco, S. Dmitrievsky, M. Dracos, D. Duchesneau, S. Dusini, T. Dzhatdoev, J. Ebert, I. Efthymiopoulos, O. Egorov, A. Ereditato, L.S. Esposito, J. Favier, T. Ferber, R.A. Fini, T. Fukuda, A. Garfagnini, G. Giacomelli, M. Giorgini, M. Giovannozzi, C. Girerd, J. Goldberg, C. Göllnitz, D. Golubkov, L. Goncharova, Y. Gornushkin, G. Grella, F. Grianti, E. Gschwendtner, C. Guerin, A.M. Guler, C. Gustavino, C. Hagner, K. Hamada, T. Hara, R. Enikeev, M. Hierholzer, A. Hollnagel, M. Ieva, H. Ishida, K. Ishiguro, K. Jakovcic, C. Jollet, M. Jones, F. Juget, M. Kamiscioglu, J. Kawada, S.H. Kim, M. Kimura, E. Kiritsis, N. Kitagawa, B. Klicek, J. Knuesel, K. Kodama, M. Komatsu, U. Kose, I. Kreslo, C. Lazzaro, J. Lenkeit, A. Ljubicic, A. Longhin, A. Malgin, G. Mandrioli, J. Marteau, T. Matsuo, V. Matveev, N. Mauri, A. Mazzoni, E. Medinaceli, F. Meisel, A. Meregaglia, P. Migliozzi, S. Mikado, D. Missiaen, P. Monacelli, K. Morishima, U. Moser, M.T. Muciaccia, N. Naganawa, T. Naka, M. Nakamura, T. Nakano, Y. Nakatsuka, D. Naumov, V. Nikitina, F. Nitti, S. Ogawa, N. Okateva, A. Olchevsky, O. Palamara, A. Paoloni, B.D. Park, I.G. Park, A. Pastore, L. Patrizii, E. Pennacchio, H. Pessard, C. Pistillo, N. Polukhina, M. Pozzato, K. Pretzl, F. Pupilli, R. Rescigno, F. Riguzzi, T. Roganova, H. Rokujo, G. Rosa, I. Rostovtseva, A. Rubbia, A. Russo, V. Ryasny, O. Ryazhskaya, O. Sato, Y. Sato, Z. Sah-

noun, A. Schembri, J. Schuler, L. Scotto Lavina, J. Serrano, I. Shakiryanova, A. Sheshukov, H. Shibuya, G. Shoziyoev, S. Simone, M. Sioli, C. Sirignano, G. Sirri, J.S. Song, M. Spinetti, L. Stanco, N. Starkov, S. Stellacci, M. Stipcevic, T. Strauss, S. Takahashi, M. Tenti, F. Terranova, I. Tezuka, V. Tioukov, P. Tolun, N.T. Trani, S. Tufanli, P. Vilain, M. Vladimirov, L. Votano, J.-L. Vuilleumier, G. Wilquet, B. Wonsak, J. Wurtz, V. Yakushev, C.S. Yoon, J. Yoshida, Y. Zaitsev, S. Zemskova, A. Zghiche: Measurement of the neutrino velocity with the OPERA detector in the CNGS beam, J. High Energy Phys. **2012**(10), 1–37 (2012)

41.8 D. Mills: *Computer Network Time Synchronization: The Network Time Protocol on Earth and in Space*, 2nd edn. (CRC, Boca Raton 2012)

41.9 D.W. Alllan, M. Weiss: Accurate time and frequency transfer during common-view of a GPS satellite, Proc. IEEE FCS 1980, Philadelphia (1980) pp. 334–356

41.10 G. Petit: The TAIPPP pilot experiment, Proc. Joint IEEE FCS and 23rd EFTF, Besançon (2009) pp. 116–119

41.11 P. Defraigne, G. Petit: CGGTTS-Version 2E: An extended standard for GNSS time transfer, Metrologia **52**(6), G1 (2015)

41.12 D.W. Allan, C. Thomas: Technical directives for standardization of GPS time receiver software, Metrologia **31**, 69–79 (1994)

41.13 J. Levine: Time transfer using multi-channel GPS receivers, IEEE Trans. Ultrason. Ferroelectr. Freq. Contr. **46**(2), 284–291 (1999)

41.14 M. Hernández-Pajares, J.M. Juan, J. Sanz, R. Orus, A. Garcia-Rigo, J. Feltens, A. Komjathy, S.C. Schaer, A. Krankowski: The IGS VTEC maps: A reliable source of ionospheric information since 1998, J. Geod. **83**, 263–275 (2009)

41.15 P. Defraigne, G. Petit: Time transfer to TAI using geodetic receivers, Metrologia **40**, 184–188 (2003)

41.16 G. Petit, Z. Jiang: GPS All in view time transfer for TAI computation, Metrologia **45**, 35–45 (2008)

41.17 M.A. Weiss, G. Petit, Z. Jiang: A comparison of GPS common-view time transfer to all-in-view, Proc. IEEE FCS, Vancouver (2005) pp. 1–5

41.18 M.C. Martínez-Belda, P. Defraigne: Combination of TWSTFT and GPS data for time transfer, Metrologia **47**, 305–316 (2010)

41.19 T. Schildknecht, G. Beutler, M. Rothacher: Towards sub-nanosecond GPS time transfer using geodetic processing technique, Proc. 4th EFTF, Neuchatel (1990) pp. 335–346

41.20 K.M. Larson, J. Levine, L.M. Nelson, T. Parker: Assessment of GPS carrier-phase stability for time-transfer applications, IEEE Trans. Ultrason. Ferroelectr. Freq. Contr. **47**(2), 484–494 (2000)

41.21 C. Bruyninx, P. Defraigne: Frequency transfer using GPS codes and phases: Short and long term stability, Proc. 31st PTTI Meet., Dana Point, ed. by L.A. Breakiron (USNO, Washington DC 2000) pp. 471–478

41.22 K. Senior, J. Ray: Accuracy and precision of carrier phase clock estimates, Proc. 33rd PTTI Meet., Long Beach, ed. by L.A. Breakiron (USNO, Washington DC 2001) pp. 199–217

41.23 J. Ray, K. Senior: Geodetic techniques for time and frequency comparisons using GPS phase and code measurements, Metrologia **42**(4), 215–232 (2005)

41.24 P. Defraigne, C. Bruyninx: Multipath mitigation in GPS-based time and frequency transfer, Proc. 20th EFTF, Braunschweig (2006) pp. 524–529

41.25 D. Orgiazzi, P. Tavella, F. Lahaye: Experimental assessment of the time transfer capability of precise point positioning (PPP), Proc. IEEE FCS, Vancouver (2005) pp. 337–345

41.26 K. Senior, E. Powers, D. Matsakis: Attenuating day-boundary discontinuities in GPS carrier-phase time transfer, Proc. 31st Precise Time Time Interval Syst. Appl. (PTTI) Meet., Dana Point (USNO, Washington DC 2000) pp. 481–490

41.27 N. Guyennon, G. Cerretto, P. Tavella, F. Lahaye: *Further characterization of the time transfer capabilities of precise point positioning* (PPP), PROCBEGINProc. Joint IEEE Freq. Contr. Symp. 21st Eur. Freq. Time Forum, GenevaPROCEND (2007) pp. 399–404

41.28 J. Delporte, F. Mercier, D. Laurichesse: Time transfer using GPS carrier phase with zero-difference integer ambiguity blocking, Proc. 22nd EFTF, Toulouse (2008) pp. 1–6

41.29 G. Petit, A. Harmegnies, F. Mercier, F. Perosanz, S. Loyer: The time stability of PPP links for TAI, Proc. Joint IEEE FCS and 25th EEFTF, San Francisco (2011) pp. 1–5

41.30 F. Lahaye, P. Collins, G. Cerretto, P. Tavella: Advances in time and frequency transfer from dual-frequency GPS pseudorange and carrier-phase observations, Proc. 40th PTTI Syst. Appl. Meet., Reston (2009) pp. 415–432

41.31 J. Ray: Systematic errors in GPS position estimates. Presentation at IGS 2006 Workshop, Darmstadt (available electronically at ftp://igscb.jpl.nasa.gov/pub/resource/pubs/06_darmstadt/IGS%20Presentations%20PDF/11_6_Ray.pdf)

41.32 W. Aerts, Q. Baire, C. Bruyninx, J. Legrand, E. Pottiaux: Towards better GNSS observations at the new IGS reference station BRUX: Multi path mitigation and individual antenna calibration, Proc. AGU Fall Meet., San Francisco (AGU, Washington 2012), abstract No. G51C–07

41.33 Q. Baire, P. Defraigne, E. Pottiaux: Influence of troposphere in PPP time transfer, Proc. Joint IEEE FCS and 23rd EFTF, Besançon (2009) pp. 1065–1068

41.34 U. Weinbach, S. Schön: On the correlation of tropospheric zenith path delay and station clock estimates in geodetic GNSS frequency transfer, Proc. 24th Eur. Freq. Time Forum, Noordwijk (2010) pp. 1–8

41.35 P. Defraigne, G. Petit, C. Bruyninx: Use of geodetic receivers for TAI, Proc. 31st PTTI Syst. Appl. Meet., Long Beach, ed. by L.A. Breakiron (USNO, Washington DC 2002) pp. 341–348

41.36 Bureau International des Poids et Mesures: Consultive Committee for Time and Frequency (CCTF) http://www.bipm.org/utils/en/pdf/CCTF15-EN.pdf

41.37 P. Defraigne, G. Petit, P. Uhrich, W. Aerts: Requirements on GNSS receivers from the perspective of timing applications, Proc. 24th Eur. Freq. Time Fo-

rum, Noordwijk (2010) pp. 1–6
41.38 J. White, R. Beard, G. Landis, G. Petit, E. Powers: Dual frequency absolute calibration of a geodetic GPS receiver for time transfer, Proc. 15th EFTF, Neuchatel (2001) pp. 167–172
41.39 G. Cibiel, A. Proia, L. Yaigre, J.-F. Dutrey, A. de Latour, J. Dantepal: Absolute calibration of geodetic receivers for time transfer: Electrical delay measurement, uncertainties and sensitivities, Proc. 22nd EFTF, Toulouse (CNES, Toulouse 2008) pp. 1–7
41.40 J. Plumb, K. Larson, J. White, E. Powers: Absolute calibration of a geodetic time transfer system, IEEE Trans. Ultrason. Ferroelectr. Freq. Contr. **52**(11), 1904–1911 (2005)
41.41 A. Proia, G. Cibiel, L. Yaigre: Time stability and electrical delay comparison of dual frequency GPS receivers, Proc. 44th Annu. PTTI Meet. (2012) pp. 297–302
41.42 G. Petit, Z. Jiang, P. Uhrich, F. Taris: Differential calibration of Ashtech Z12-T receivers for accurate time comparisons, Proc. 14th EFTF, Torino (Swiss Foundation for Research in Microtechnology, Neuchâtel 2000) pp. 40–44
41.43 H. Esteban, J. Palacio, F.J. Galindo, T. Feldmann, A. Bauch, D. Piester: Improved GPS-based time link calibration involving ROA and PTB, IEEE Trans. Ultrason. Ferroelectr. Freq. Contr. **57**(3), 714–720 (2010)
41.44 M. Weiss, F. Ascarrunz, T. Parker, V. Zhang, X. Gao: Effects of antenna cables on GPS timing receivers, Proc. Joint IEEE FCS and 13th EFTF, Besançon (1999) pp. 259–262
41.45 G. Petit, P. Defraigne, B. Warrington, P. Uhrich: Calibdation of sual frequency GPS receivers for TAI, Proc. 20th EFTF, Braunschweig (PTB, Braunschweig 2006) pp. 455–459
41.46 T. Feldmann, A. Bauch, D. Piester, M. Rost, E. Goldberg, S. Mitchell, B. Fonville: Advanced GPS-based time link calibration with PTB's new GPS calibration setup, Proc. 42nd PTTI Syst. Appl. Meet., Reston (2011) pp. 509–526
41.47 D. Rovera, J.-M. Torre, R. Sherwood, M. Abgrall, C. Courde, M. Laas-Bourez, P. Uhrich: Link calibration against receiver calibration: An assessment of GPS time transfer uncertainties, Metrologia **51**(5), 476–490 (2014)
41.48 S.F. Adam: *Microwave Theory and Applications*, 2nd edn. (Prentice Hall, Upper Saddle River 1969)
41.49 J. Ray, K. Senior: Temperature sensitivity of timing measurements using Dorne Margolin antennas, GPS Solutions **2**(1), 24–30 (2001)
41.50 A. Smolarsk, A. Lisowiec, J. Nawrocki: Improving the accuracy of GPS time transfer by thermal stabilization of GPS antenna and receiver, Proc. 16th EFTF, St. Petersburg (Swiss Foundation for Research in Microtechnology, Neuchâtel 2002) pp. 503–505
41.51 P. Defraigne, C. Bruyninx: On the link between GPS pseudorange noise and day-boundary discontinuities in geodetic time transfer solutions, GPS Solutions **11**(4), 239–249 (2007)
41.52 M. Weiss, W. Lewandowski, P. Uhrich, D. Valat: NIST and OP GPS receiver calibrations spanning twenty years: 1983–2003, Proc. 18th EFTF, Guilford (Univ. of Surrey, Surrey 2004) pp. 143–146
41.53 A. Harmegnies, P. Defraigne, G. Petit: Combining GPS and GLONASS in all-in-view for time transfer, Metrologia **50**(3), 277–287 (2013)
41.54 P. Defraigne, Q. Baire: Combining GPS and GLONASS for time and frequency transfer, Adv. Space Res. **47**(2), 265–275 (2011)
41.55 P. Defraigne, W. Aerts, A. Harmegnies, G. Petit, D. Rovera, P. Uhrich: Advances in multi-GNSS time transfer, Proc. Joint IEEE FCS and EFTF 2013, Prague (2013) pp. 508–512
41.56 P. Defraigne, W. Aerts, G. Cerretto, G. Signorile, E. Cantoni, I. Sesia, P. Tavella, A. Cernigliaro, A. Samperi, J.M. Sleewaegen: Advances on the use of Galileo signals in time metrology: Calibrated time transfer and estimation of UTC and GGTO using a combined commercial GPS-Galileo receiver, Proc. PTTI Syst. Appl. Meet. (2014) pp. 256–262
41.57 W. Guang, H. Yuan: The application of smoothed code in BeiDou common view, Proc. CSNC 2013, Wuhan, Vol. I, ed. by J. Sun, W. Jiao, H. Wu, C. Shi (Springer, Berlin 2013) pp. 269–278
41.58 J. Furthner, A. Moudrak, A. Konovaltsev, J. Hammesfahr, H. Denks: Time dissemination and common view time transfer with galileo: How accurate will it be?, Proc. 35th Annu. PTTI Meet., San Diego (2004) pp. 185–198
41.59 A. Simsky, D. Mertens, J.M. Sleewaegen, W. De Wilde, S. Navigation, M. Hollreiser: Multipath and tracking performance of Galileo ranging signals transmitted by GIOVE-B, Proc. ION GNSS 2008, Savannah (ION, Virginia 2008) pp. 1525–1536
41.60 W.K. Yang, H. Gong, Z.J. Liu, Y.L. Li, G.F. Sun: Improved two-way satellite time and frequency transfer with multi-GEO in BeiDou navigation system, Sci. China Inf. Sci. **57**(2), 1–15 (2014)
41.61 A. Bauch, J. Achkar, S. Bize, D. Calonico, R. Dach, R. Hlavac, L. Lorini, T. Parker, G. Petit, D. Piester, K. Szymaniec, P. Uhrich: Comparison between frequency standards in Europe and the USA at the 1015 uncertainty level, Metrologia **43**, 109–120 (2006)
41.62 W. Meng, H. Zhang, P. Huang, J. Wang, Z. Zhang, Y. Liao, Y. Ye, W. Hu, Y. Wang, W. Chen: Design and experiment of onboard laser time transfer in Chinese Beidou navigation satellites, Adv. Space Res. **51**(6), 951–958 (2013)